PHASE PLUG MODELLING AND ANALYSIS:

RADIAL VERSUS CIRCUMFERENTIAL TYPES

preprint no. 1328 (F-5)

By

Clifford A. Henricksen, Altec, Anaheim, California

**presented at the
59th Convention
February 28. – March 3. 1978
Hamburg**

AES

AN AUDIO ENGINEERING SOCIETY PREPRINT

PHASE PLUG MODELLING AND ANALYSIS: RADIAL VS. CIRCUMFERENTIAL TYPES

by Clifford A. Henricksen

Altec Corporation; Anaheim, California

ABSTRACT

Mechanical modelling of a simple two-dimensional phase plug-and diaphragm yields an electrical-mobility equivalent circuit; a two-pole low-pass filter. At higher frequencies, this analysis becomes incomplete, and a model presented by Merhaut (1975) is used. These impedance models are then applied as differential elements to a radial-slit phase plug[1] geometry and its aggregate impedance is found. Actual and theoretical comparative performance is presented.

INTRODUCTION

My introduction to the analysis of phase plug performance was initiated by reviewing the "...High Frequency Receiving Unit" portion of Loudspeakers and Microphones by E. C. Wente and A. L. Thuras, circa 1934. The analysis is based on equations derived from a velocity potential function and the result is a solution for normalized throat impedance, broken into real and imaginary parts. This was all very elegant and mathematically quite reasonable. What I really needed, however, was an equivalent circuit representing the phase plug as an acoustic filter. Its characteristics could then be lumped into discrete elements for ease of analysis and for a better understanding of how the elements interacted with the rest of the driver. This, then, was the goal of the analytic investigation.

ANALYSIS

Figure (1) shows a typical circumferential-slit phase plug with path length ℓ_D shown. Its surface is spherical and the mating diaphragm sits above it at a distance "h".

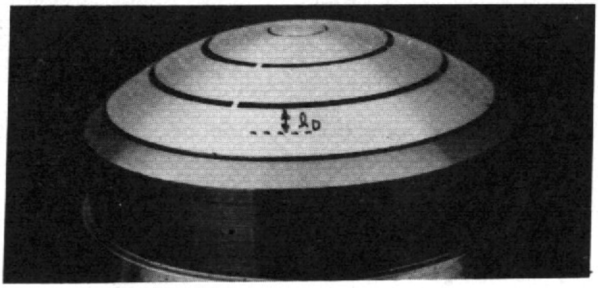

Figure (1) - Circumferential-Slit Phase Plug

[1]U.S. Patent #4050541, foreign patents pending

Figure (2) shows a simplification of Figure (1), as presented in Wente and Thuras' original paper.

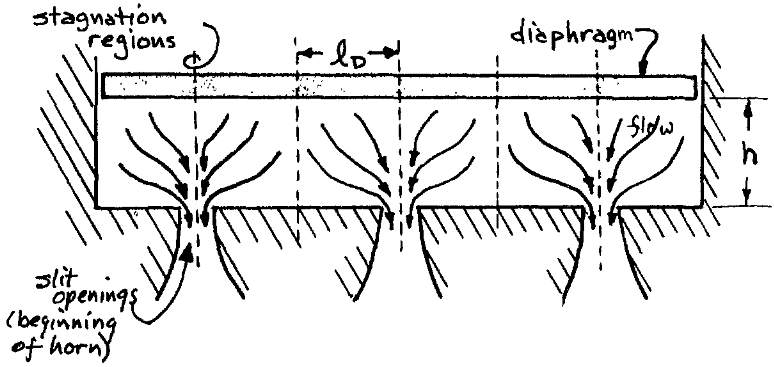

Figure (2) - Simplification of Circumferential Phase Plug.

If ℓ_D is too big, a high frequency cancellation is known to occur at some frequency determined by this dimension. Therefore, we should design the phasing plug with ℓ_D as small as possible, necessitating a lot of air channels for passage of high frequencies. Figure (3) is a simplification of a section of diaphragm and throat between "stagnation" points (dotted lines in Figure (2)) which are imaginary boundaries over which no air flow occurs. These can be considered as rigid boundaries.

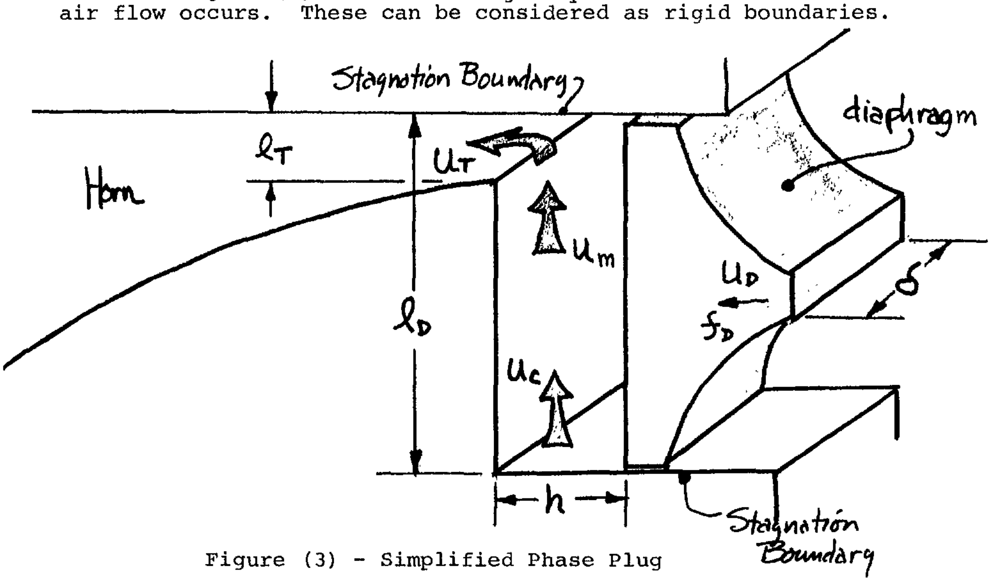

Figure (3) - Simplified Phase Plug

where

ℓ_T = throat width
U_T = throat velocity
U_C = air velocity under diaphragm
U_M = velocity of air mass under diaphragm near throat
ℓ_D = diaphragm dimension
U_D = diaphragm velocity
f_D = diaphragm force
h = diaphragm-to-phase plug spacing
δ = diaphragm width

The air space under the diaphragm possesses compressibility as well as inertia. As a result, a single frequency resonant condition is possible, its vibration being parallel to the diaphragm. Velocity U_C will differ from U_M due to compressibility. Velocity U_T will differ from U_M due to the acoustic transformer (h/ℓ_T). Figure (4) is an equivalent mechanical circuit describing the operation of Figure (3) and should be clear in its derivation.

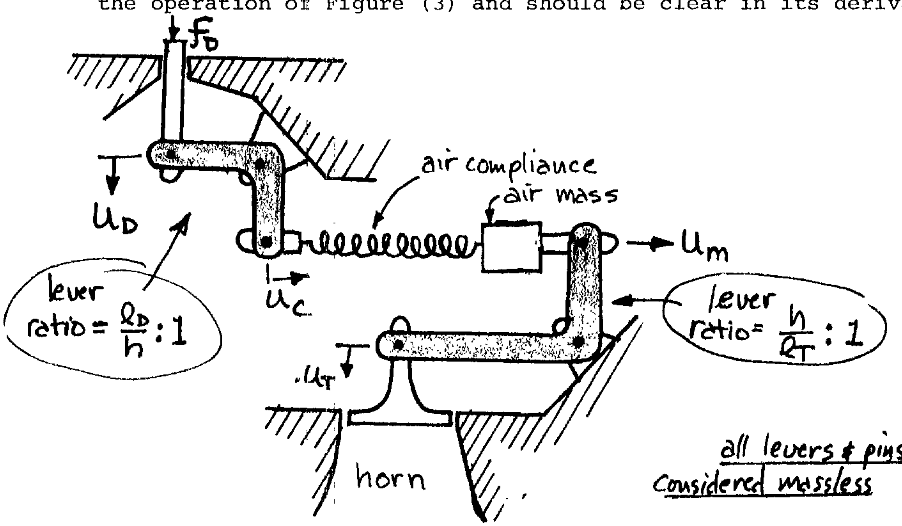

Figure (4) - Mechanical Circuit Equivalent of Figure (3)

An electrical impedance equivalent circuit of the diaphragm-phase plug can now be made. Performance of this circuit will be later compared with Wente and Thuras' results and the circuit will be transformed to a mobility circuit for a complete driver model. The compliance under the phase plug is found by normal equations keeping in mind the flow direction. The mass under the phase plug is its "equivalent" mass and is numerically one-third of the total air mass[1]. This equivalent circuit is shown in Figure (5). Compare it to Figures (3) and (4).

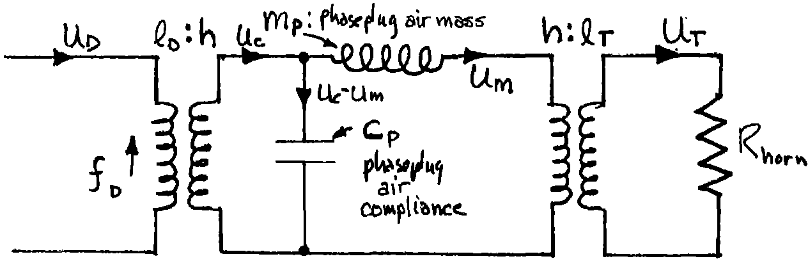

Figure (5) - Phase Plug Mechanical-Impedance Equivalent Circuit

Removing transformers by using appropriate constants yields the following circuit shown in Figure (6):[2]

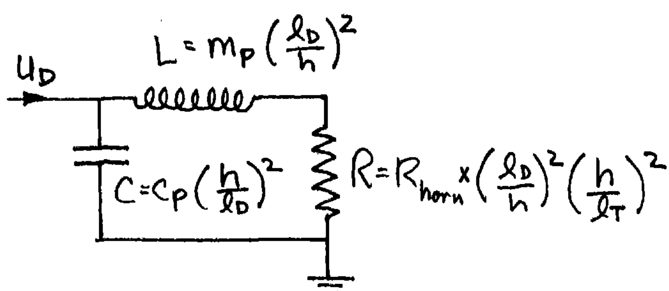

Figure (6) - Transformed Phase Plug Circuit

where m_p is the effective mechanical mass of the phase plug air cavity;

$$m_p = \frac{\rho \times \text{volume}}{3} = \frac{\rho_0 \delta h l_D}{3} = \frac{\rho_0 \delta h S_D}{3} \qquad (1)$$

[1] See Appendix 1 for proof.
[2] Other resistances are present here, but are deemed insignificant. See Appendix 2.

c_p = the effective mechanical compliance of the phase plug air cavity;

$$c_p = \frac{\text{volume}}{\rho_0 C^2 S^2} \quad \text{"S" is area normal to flow } (h\delta)$$

So

$$c_p = \frac{l_D \delta h}{\rho_0 c^2 (h\delta)^2} = \frac{l_D}{\rho_0 C^2 \delta h} \tag{2}$$

Therefore, from Figure (6), the final mechanical-impedance circuit will have the following values for R, L and C;

$$R = \rho_0 C S_T \left(\frac{l_D}{l_T}\right)^2 = \frac{\rho_0 c \delta l_D^2}{l_T} \tag{3}$$

$$C = m_P \left(\frac{h}{l_D}\right)^2 = \frac{\rho_0 h^3 \delta}{3 l_D} \tag{4}$$

$$L = C_P \left(\frac{l_D}{h}\right)^2 = \frac{l_D^3}{\rho_0 C^2 \delta h} \tag{5}$$

Figure (6) should be easily recognized as a simple two-pole low-pass circuit. Its input impedance can be solved for real (Re) and imaginary (Im) parts as follows:

$$Z = \frac{j\omega L + R}{1 - \omega^2 LC + j\omega RC} \tag{6}$$

Using standard complex algebra and defining

$$\Omega^2 \equiv \omega^2/\omega_0^2 = \omega LC \tag{7}$$

$$K \equiv \frac{(RC)^2}{\omega_0^2} = \frac{R^2 C}{L} \tag{8}$$

We arrive at normalized equations

$$\frac{Re}{R} = \frac{1}{1 + (K-2)\Omega^2 + \Omega^4} \tag{9}$$

$$\frac{Im}{R} = j\frac{\Omega \frac{(1-K)}{\sqrt{K}} - \frac{\Omega^3}{\sqrt{K}}}{1 + (K-2)\Omega^2 + \Omega^4} \tag{10}$$

Using (3), (4) and (5) in (8) yields

$$K = \frac{3h^2}{\ell_T^{\,2}} \quad \text{or} \tag{11}$$

$$\frac{h}{\ell_T} = \sqrt{\frac{K}{3}} \tag{12}$$

Figure (7) shows the results of Wente and Thuras, noting that W&T's "h/w" is the same as our "h/ℓ_T." The impedance shown are normalized with respect to the referred horn resistance $\rho_0 CAT^2$, which is identical to those impedances in (9) and (10).

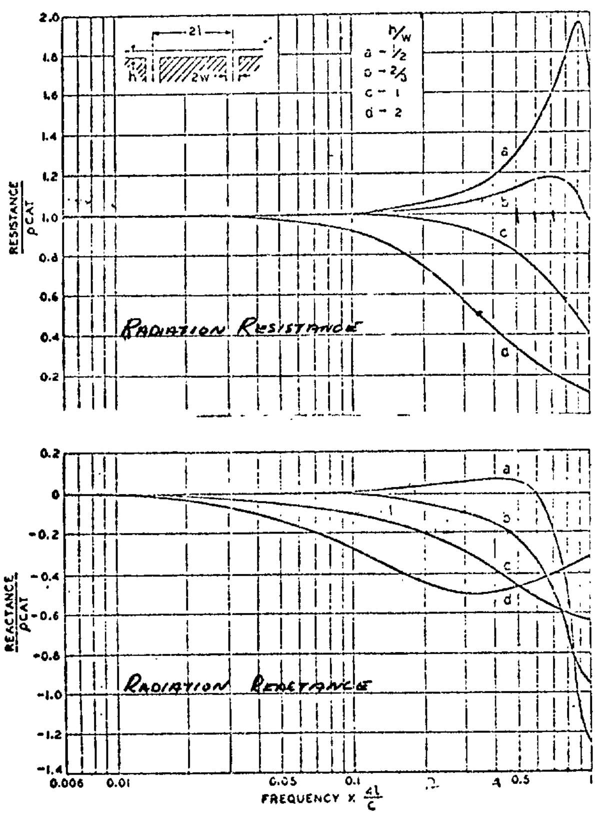

Figure (7) - Wente and Thuras' Results:
Diaphragm Impedance

Now, compare this to results obtained from our equations (9) and (10). From equation (11), Wente and Thuras' "h/w" of 1/2, 2/3, 1 and 2 correspond to our "K" values of .75, 1.333, 3 and 12 respectively. Our frequency scale corresponds to a greater-than-quarter wavelength by using

$$f_o = \frac{1}{2\pi\sqrt{LC}} \tag{13}$$

Using (4) and (5) in (13) yields

$$f_o = \frac{\sqrt{3}\,c}{2\pi \ell_D} = \frac{c}{3.63\,\ell_D} \tag{14}$$

So our frequency scale is shifted by a factor of 4/3.63 or a factor of 1.102 higher. Comparing curves of our results, shown in Figure (8), next page, we see very close agreement to $\Omega=1$, which is where the Wente and Thuras analysis stops.

At higher frequencies ($\Omega>1$) this model becomes too simple, as the air under the diaphragm goes into a more "discrete" vibrational behavior. Merhaut has taken the analysis a step further and suggested a high-frequency model which appears in impedance form in Figure (9). Merhaut's equivalent circuit is cleverly derived from the form of the transfer function he derives from the wave equation.

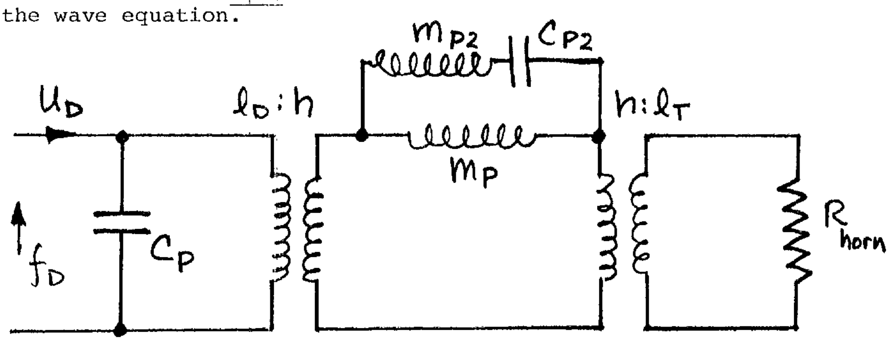

Figure (9) - Merhaut High Frequency Phase Plug Impedance Model

where

M_{P2} is a second-order mass

C_{P2} is a second-order compliance

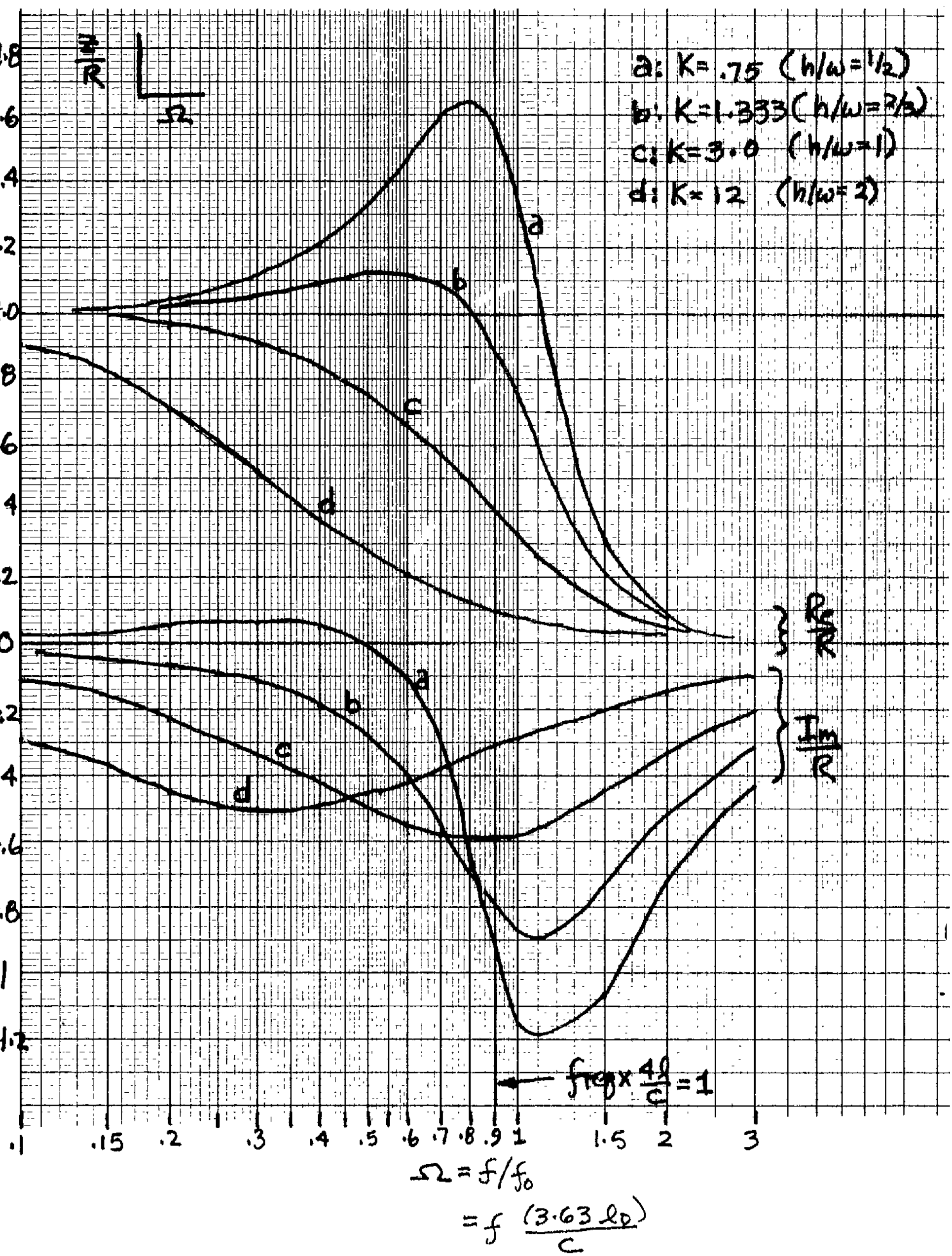

Figure (8) - Normalized Mechanical Diaphragm Impedance, derived from equations (10) and (11), for simple two-pole model

Figure (9) can be simplified (transformers removed) to the circuit shown in Figure (10).

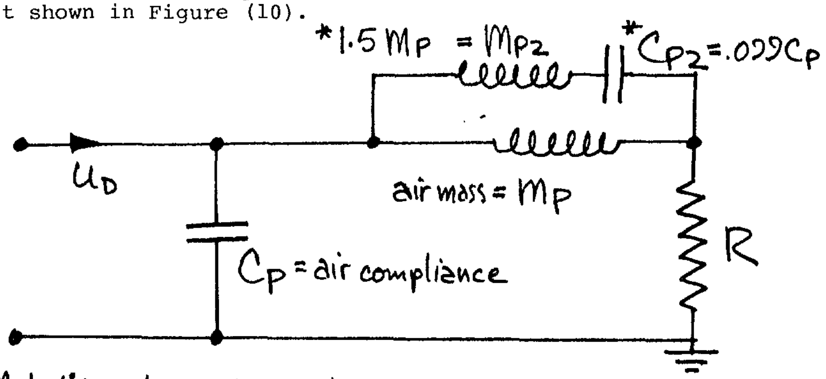

*from Merhaut, $M_{p2} = \frac{1}{2} M_{tot}$; but $M_p = \frac{1}{3} M_{tot}$ $\therefore$ $M_{p2} = \frac{3}{2} m_p$

Figure (10) - Transformed Merhaut Equivalent Impedance Model

Compare Figure (10) to Figure (6) and note that the only difference is the "L-C" added across the inductor representing mass. Upon inspection of Merhaut's paper, it was (encouragingly) found that the equivalent "first-mode" compliance and air mass for both analyses agreed. It turned out, conveniently, that the second-order elements could be expressed as follows:

$$C_{\rho 2} = .099C_{\rho} \tag{15}$$

$$M_{\rho 2} = 1.5M_{\rho} \tag{16}$$

A mobility equivalent circuit for Figure (9) is as follows in Figure (11):

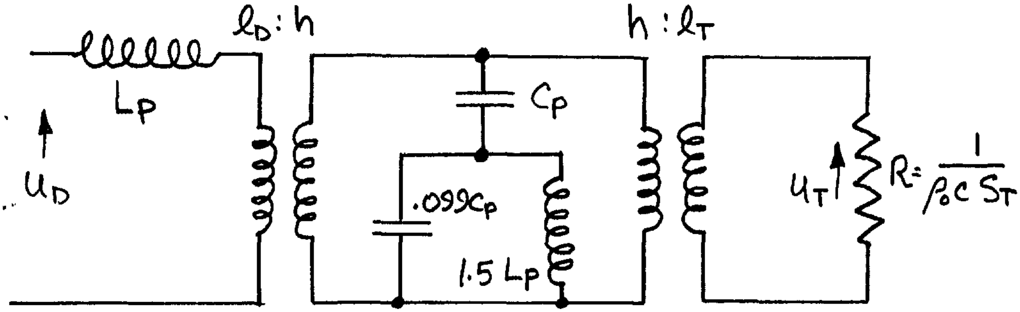

Eliminating transformers by ratio multiplication yields the following mobility circuit shown in Figure (12).[1]

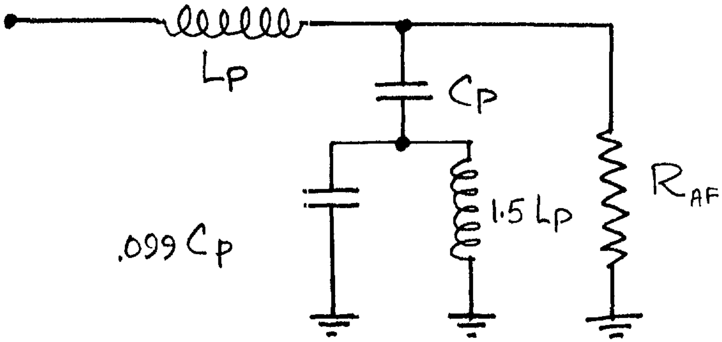

Figure (12) - Transformed Equivalent of Figure (11) and Final Mobility Phase Plug Model

where $$L_\rho = \frac{l_D}{\rho_0 c^2 \delta h} \cdot \frac{h^2}{l_D^2} = \frac{h}{\rho_0 c^2 \delta l_D} \approx \frac{h}{\rho_0 c^2 S_D} \qquad (17)$$

from (1) $$C_\rho = \frac{\rho_0 h S_D}{3} \cdot \frac{l_D^2}{h^2} = \frac{\rho_0 S_D l_D^2}{3h} \qquad (18)$$

$$R_{AF} = \frac{1}{\rho_0 c S_T} \cdot \frac{l_T^2}{h^2} = \frac{S_T}{\rho_0 c S_D^2} \qquad (19)$$

The transfer function of Figure (12) can be solved for response, R.

$$R \equiv \frac{e_{out}}{e_{in}} = \frac{1 - .2475\,\Omega^2}{(j/\sqrt{K})(\Omega - .2475\,\Omega^3) + 1 - 1.2475\,\Omega^2 + .1485\,\Omega^4} \qquad (20)$$

where the variables Ω and K are as per equations (7) and (8). Equation (20) is plotted to $\Omega=3$ in Figure (14). Compare it to Figure (8).

[1] These models and the next higher order circuit suggested by Merhaut were all examined analytically. Except for a small depth-of-notch, the higher order models are identical to $\Omega=3$. The performance of the simple two-pole low-pass and Merhaut's model in Figure (10) are identical to $\Omega=1$.

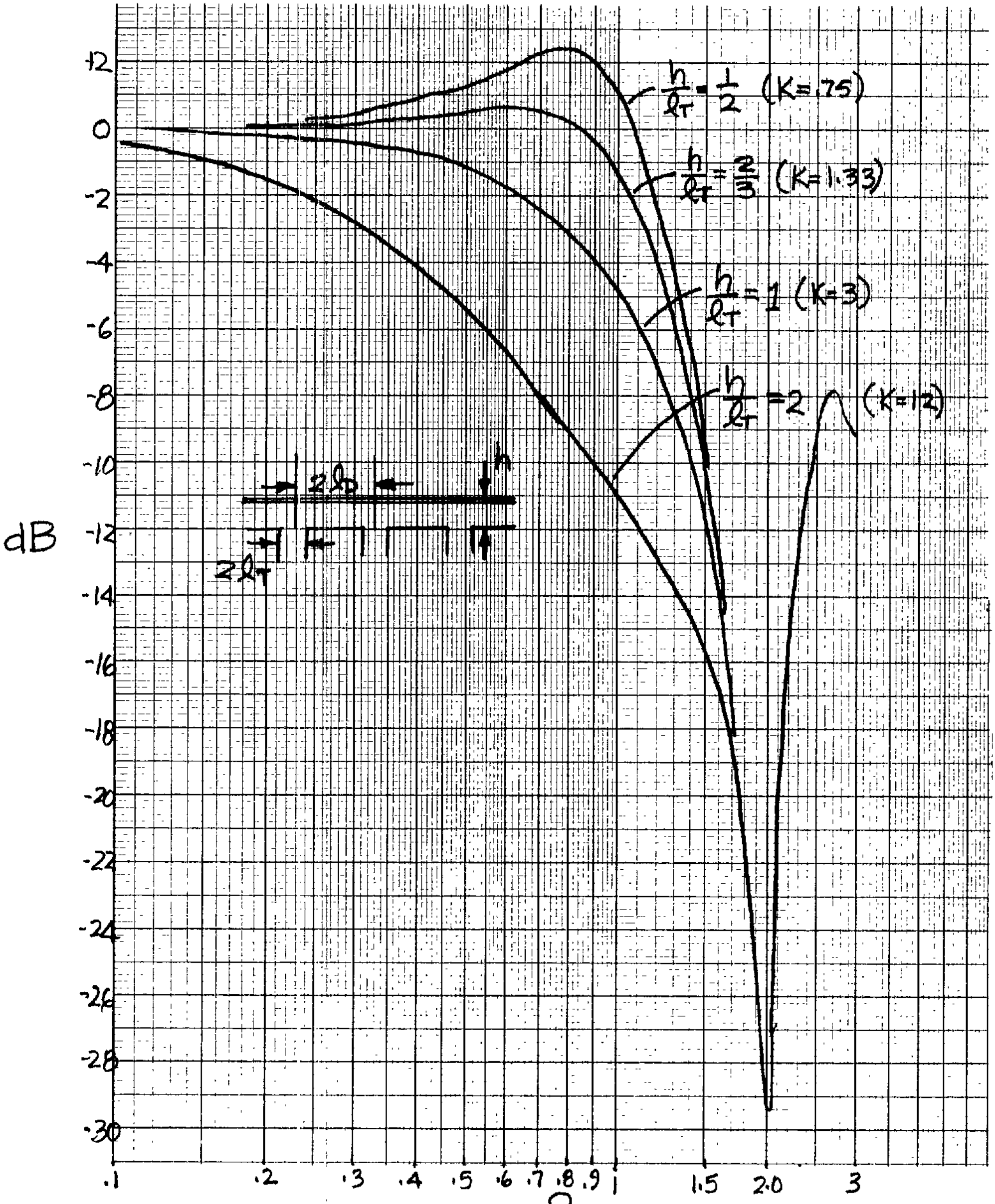

Figure (14) - Normalized Response of Single-Path Phase Plug, per equation (20)

As a final model of the entire driver, Figure (12) can be added to a standard high frequency driver mobility model. This is shown in Figure (15).

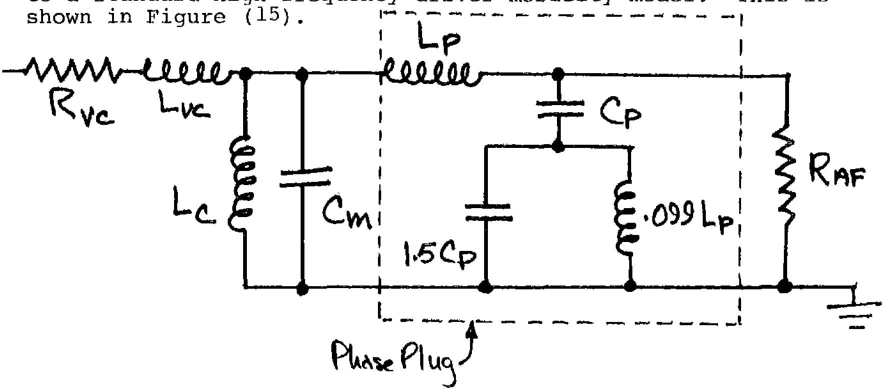

Figure (15) - Complete Driver Model Including Circumferential Phase Plug

where

R_{VC}	=	voice coil resistance	
L_{VC}	=	voice coil inductance	
C_m	=	capacitor representing total diaphragm mass $= M_T/(B\ell)^2$	(21)
L_C	=	inductor representing suspension compliance $= B^2\ell^2 C_T$	(22)
R_{AB}	=	back diaphragm radiation resistance $= (B\ell)^2/\rho o C S_D$	(23)
C_p	=	capacitor representing phase plug mass $= \rho o S_D \ell_D{}^2/3(B\ell)^2 h$	(24)
L_p	=	inductor representing phase plug compliance $= (B\ell)^2 h/\rho o C^2 S_D$	(25)
R_{AF}	=	horn radiation resistance $= (B\ell)^2 S_T/\rho o C S_D^2$	(26)

<u>RADIAL-SLIT PHASE PLUG</u>

Figure (16) on the next page shows a radial phase plug, maximum ℓ_D being indicated.

The radial slit configuration differs from the circumferential type by having ℓ_D decrease toward the center. The effect of spacing between the diaphragm and phase plug is the same for both types of phase plugs; this results from the air reactance

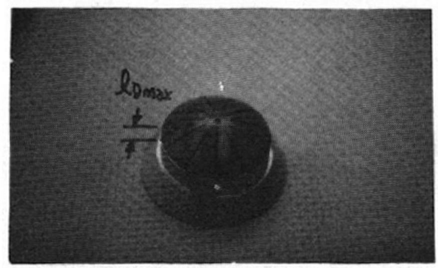

Figure (16) - Radial Phase Plug

(compliance) shown as L_p in the mobility circuit and is found by equation (25). Note that it is independent of ℓ_D. Hence, the only difference between radial and circumferential types should be the "effective" air mass C_p; if ℓ_D was zero, C_p would be zero and the air in the phase plug would be massless.

Let's look at a radial phase plug. Figure (17) shows a small section with a small portion of the diaphragm (dr) wide at distance r from the center.

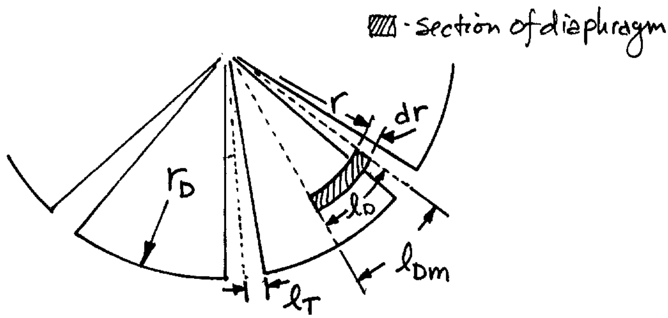

Figure (17) - Radial Phase Plug Close-up

Clearly, arc ℓ_D varies from zero to ℓ_{Dm} at the O.D., according to the relationship.

$$\ell_D = \frac{\ell_{Dm} r}{r_D} = \ell_{Dm} P \tag{27}$$

where $P = r/r_D$ (28)

arc ℓ_{Dm} or max ℓ_D is

$$\ell_{Dm} = \frac{2\pi r_D}{2N} = \frac{\pi r_D}{N} \tag{29}$$

where N is the number of slits.

Also, for this example, the slits are tapered, having a maximum width of $(2\ell T_m)$ at the periphery. Therefore, similar to (29)

$$\ell T = \frac{\ell_{Tm} r}{r_D} = \ell_{Tm} P \tag{30}$$

In this stage of the analysis, we should note that for the inner portions of the diaphragm, the resonant frequency is high, but since the relative damping is constant, the "Q" of these sections is low. The outer sections would be higher "Q" but resonate at lower frequency. The net result will be an aggregate of all these impedances. The plan will be to find a "bulk" or lumped-parameter mechanical model which describes the behavior of this device.

Our typical differential diaphragm segment can be represented by Figure (12). Since different acoustic powers will be generated in each of the differential elements, a summation of all these powers should give the total power response. The transfer function for any differential element is given by equation (20). Since the normalized frequency, Ω, varies with dimension ℓ_D, let us say that Ω will be determined by ℓ_D max, as in equation (14). Therefore, local Ω will be ΩP, per equation (27). Also, local "K", per equation (11) will become KP^2. Then, per equation (20), the transfer function of our differential element will become

$$R_{radial} \equiv \frac{e_{out}}{e_{in}} = \frac{1 - .2475\Omega^2 P^2}{\frac{j}{\sqrt{K}}(\Omega - .2475\Omega^3 P^2) + 1 - 1.2475\Omega^2 P^2 + .1485\Omega^4 P^4} \tag{31}$$

A normalized power response, W, is found as follows;

$$W = \frac{\sum \text{all local powers}}{\text{Assymptotic power out}} = \frac{\sum e_{local}^2 / R_{local}}{e_{in}^2 / R_{total}} \tag{32}$$

from (3), inverting for mobility,

$$R_{local} = \frac{\ell_{Tm}}{\rho_0 c\, \ell_{Dm}^2 P dr} \tag{33}$$

and $$R_{total} = \frac{2\, l_{Tm}}{\rho_o C\, l_{Dm}^2\, r_D} \tag{34}$$

therefore, from (32), (33) and (34)

$$W = \sum \left(\frac{e_{local}}{e_{in}}\right)^2 \frac{R_{total}}{R_{local}} = \sum \left(\frac{e_{local}}{e_{in}}\right)^2 (2\,P\,dP) \tag{35}$$

from (31), therefore,

$$W = 2\sum_{n=1}^{N} \left| \frac{1 - .2475\Omega^2 P^2}{\frac{1}{\sqrt{K}}(\Omega - .2475\Omega^3 P^2) + 1 - 1.2475\Omega^2 P^2 + .1485\Omega^4 P^4} \right|^2 P\Delta P \tag{36}$$

Equation (36) was solved by dividing the normalized radius into 100 parts, therefore N=100, ΔP=.01 and P=N(.01). This was done on a computer and solved as a 10 log function for response in dB. The results are in Figure (18) on the next page.

COMPARISON OF THEORETICAL PERFORMANCE

We can show that for the same throat area (hence resistance) and the same maximum path length, the maximum throat width will be the same.[1] A real-life circumferential-plug driver has an ℓ_D of about 1/4" which places Ω=1 at 13.4 kHz, per equation (14). For the same driver diaphragm spacing, h, and slit area, we would like to compare the performance of just the phase plug to a substitute radial design. Both would operate at ℓ_T/ℓ_D = (.70). From Figures (14) and (18) we can evaluate the relative performance of the two phase plugs. This is shown in Figure (19). At once we can see the theoretical difference between the two phase plug types. The first is that the radial is a much "lower Q" kind of filter with a more gradual roll-off and without a severe notch at the high end. Theoretically we would expect a 5 dB gain at 20 kHz and a 1.2 dB loss around 9.4 kHz due to the radial's lack of "bump" at these frequencies. The lack of a discrete notch can be seen at all spacings "h" when comparing Figures (14) and (18). This is attributed to the "distributed" nature of the radial flow path, as opposed to the "discrete" single-path behavior of the circumferential; the radial plug has an infinite variety of flow path lengths and the circumferential has only one. Of interest is constant-width radial slits. Analysis of this configuration would be quite difficult, but it lends itself better to manufacture. In practice, it has been observed that for the same ℓ_D max and total throat area, tapered-slit and straight-slit radial phase plugs exhibit identical behavior.

[1] See Appendix (3)

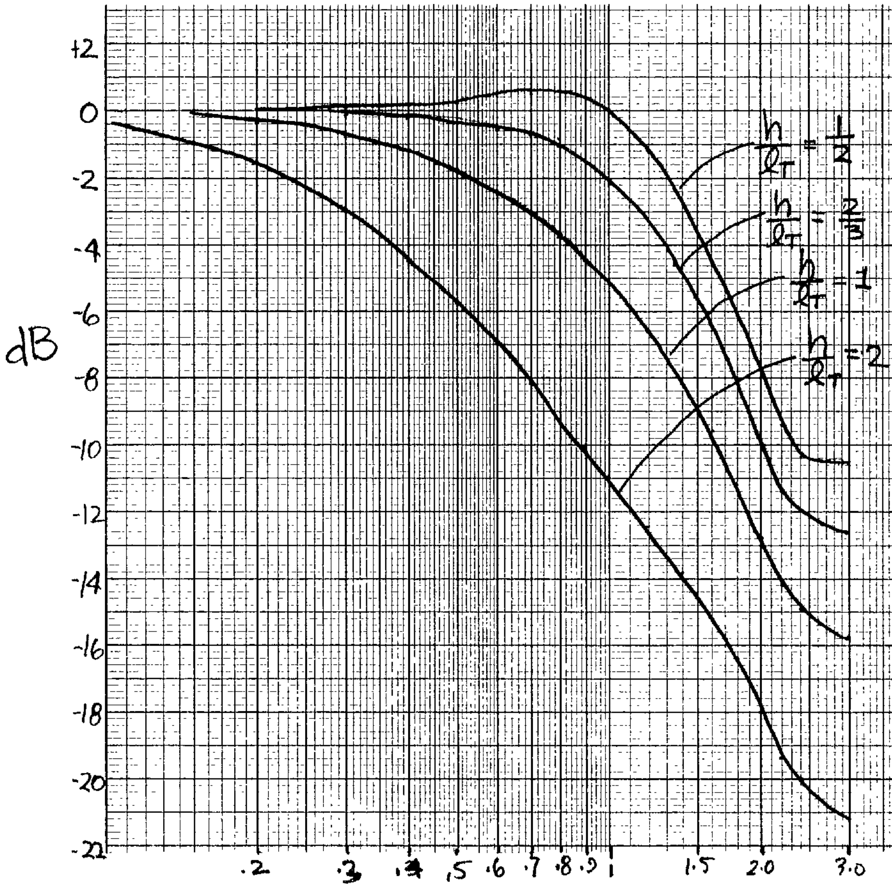

Figure (18) - Normalized Response of Radial-Slit Phase Plug

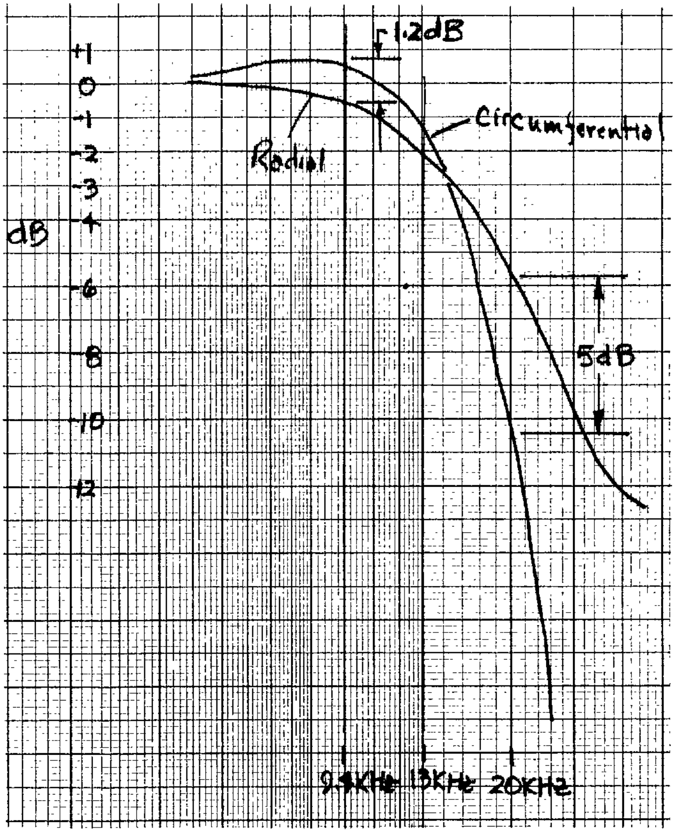

Figure (19) - Theoretical Comparative Responses of Radial and Circumferential Designs

COMPARISON OF REAL PERFORMANCE

A radial phase plug, as discussed in the previous paragraph, was designed to replace an existing circumferential design. Increased performance is always desirable, but if it were identical in performance, it would be much more attractive, since it could be single-piece injection molded. The current circumferential design is very expensive to manufacture. The two designs employed a 1.75" diaphragm-and-voice coil. Tests were performed on a typical exponential horn. The on-axis response of the radial driver was equalized as flat as possible (Altec 1620 1/3-octave equalizer) and then the circumferential unit was substituted, using the same diaphragm and E.Q. settings. Care was taken to keep diaphragm spacing, "h", the same. Also, magnetic assemblies were selected for identical gap flux so that only phase plug performance could be evaluated. These curves are shown in Figure (20).

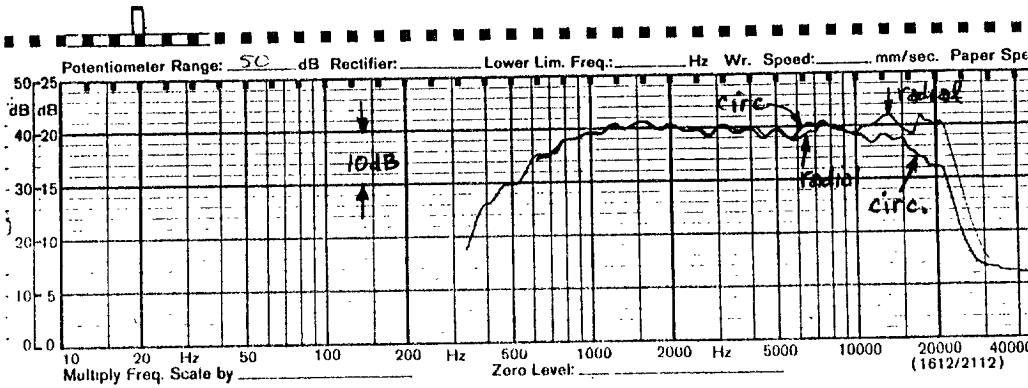

Figure (20) - Actual Response of Drivers
(both with same E.Q.)

DISCUSSION

Actual performance is somewhat close to predicted, with a final gain of about 8 dB at 20 kHz and something like a 1 dB loss in the high mid-region (6-7 kHz). It seems as if the entire analysis would be closer if it were lower in frequency, i.e., $\Omega=1$ would occur at a lower frequency theoretically. This means a shift of frequency by a factor of 1.2 lower. Also not taken into consideration is the way the geometry of the phase plug affects the breakup modes of the diaphragm. The radial phase plug shown was designed to have a prime number of slits (11) and, depending on the position of modes in the diaphragm relative to the phase plug slits, flow may be affected in different ways. Obviously, an inclusion of this into the analysis would be very difficult!

CONCLUSION

A phasing plug in a high frequency compression driver is modeled as a two-pole low-pass filter, its resonant frequency being determined by the mass and compliance of the air between the diaphragm and the phase plug. This model seems to be accurate up to its resonant frequency. Above this, a model suggested by Merhaut is used, which includes the higher-mode vibration behavior of the phase plug air, and its frequency range seems accurate to three times the first-mode resonance. This model is used as a differential element for analysis of a radial-slit phase plug, which is shown to be a relatively lower-Q filter. Due to its "distributed" multi-path length geometry, the radial phase plug exhibits a much smoother "spread-out" response compared to a "conventional" circumferential design, which is shown to notch very severely, due to its single-path geometry. For these reasons, however, a lumped-parameter model for the radial design seems unattainable since its performance is infinitely variable. This seems to make the radial design more well-suited for extended-range response. Lastly, because of its one-price castability, the radial design has a further advantage in its ease and economy of manufacturability.

The Author wishes to thank Dr. Richard Small, Prof. Dean Karnopp (U. C. Davis), John Gilliom (Spider), Jerry Siciliano (Altec) and Mark Ureda (Altec) for their contributions to this work.

BIBLIOGRAPHY

Beranek, Leo L., Acoustics, pp 262-266, (McGraw-Hill Book Co., New York, 1954)

Henricksen, Clifford A., "Ultimate Performance of Wide-Range High Frequency Compression Drivers" (presented at the 54th Convention of the Audio Engineering Society, May 4-7, 1976, Los Angeles, California)

Wente, E. C. and Thuras, A. L., "Loud Speakers and Microphones" (presented in the Symposium on Wire Transmission of Symphonic Music and Its Reproduction in Auditory Perspective, Winter Convention of A.I.E.E., Jan. 23-26, 1934, New York City)

Merhaut, J. and Skvor, Z., "An Analog Network of a Cavity Below the Diaphragm in Electro-Acoustic Transducers" - Monitor-Proceedings of IREE (Australia) Vol. 37, No. 3

Appendix (1)

A distributed spring-mass system in vibration can be modelled as a discrete system by reasoning applied to the following figures:

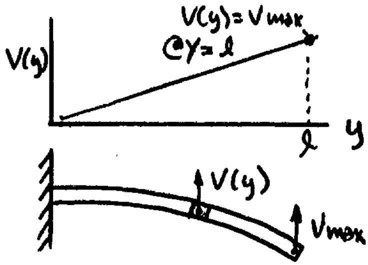

(a) Cantilever Spring

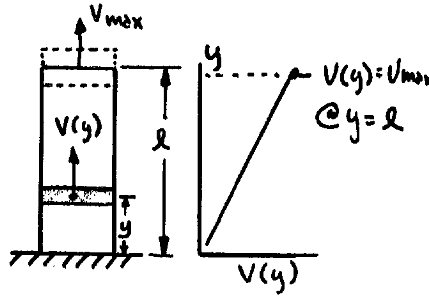

(b) Linear Vibration

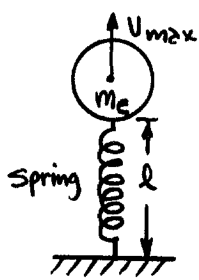

(c) Discrete Equivalent

Figure (21) - Distributed & Discrete Vibrating Systems

Both figures (a) and (b) have a linear velocity gradient with Y, V (y). Each cross-section has an area (normal to "y") whose value is "A" and a thickness dy. The material in each has a mass density ρ. The spring constant (or rate) of both, when forced in the direction of vibration is discrete; the mass is not, and the effective mass is found as a percentage of the total mass--by its contribution to the total kinetic energy of the unit. This is found by integrating the kinetic energies of all dy section.

Appendix (1) Contd.

$$V(y) = V_{MAX} \frac{Y}{\ell} \tag{37}$$

$$KE = \int_{o}^{\ell} dKE = \int_{o}^{\ell} \frac{1}{2} V^2 dm = \frac{1}{2} \int_{o}^{\ell} \frac{V^2{}_{max} Y^2}{\ell^2} \rho A dy \tag{38}$$

$$KE = \frac{1}{2} V_{MAX}{}^2 \frac{\rho A \ell}{3} = \frac{1}{2} M_e V_{MAX}{}^2 \tag{39}$$

Where M_e is the effective mass. Since the total mass, M_T, is:

$$M_T = \rho A \ell \tag{40}$$

It takes no great mathematical wizard to conclude that;

$$M_e = 1/3 \; M_T$$

Appendix (2)

Taken directly from Beranek;

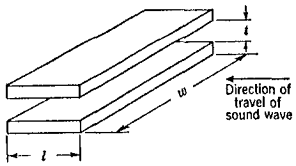

Figure (22) - Slit Resistance from Beranek

Beranek's equation (5.52) can be related to Figure (22);

Beranek's "t" = our "h"

Beranek's "w" = our "δ"

Beranek's "ℓ" = our "ℓ_D"

$$\eta = 1.86 \times 10^{-5} \eta t/m^2\text{-sec}$$

in which case our equation becomes;

$$R_P = \frac{12\eta \ \ell_D \delta}{h} \quad \text{mechanical MKS ohms} \qquad (41)$$

Taking into account the (ℓ_D/h) acoustic transformer and that this resistance is, in mobility, in common (thus in parallel) with the phase plug mass and compliance volume flow, we arrive at the following mobility electrical phase plug resistance;

$$R_P = \frac{(\beta\ell)^2 h^3}{12\eta\ell_D{}^3\delta} = \frac{(\beta\ell)^2 \ h^3}{12\eta\ell_D{}^2 S_D} \quad \text{ohms} \qquad (42)$$

This resistance appears as viscous drag along the sides of the air channel (between phaseplug and diaphragm) and "looks like" a mobility resistor from U_C' to ground. On a typical 8Ω, high efficiency driver, this calculates to about 260Ω and is judged insignificant relative to R_{AF} which is about 8Ω.

Appendix (3)

Proof: For equal ℓ_D's and total slit area, the maximum slit width for circumferential and radial phase plugs are identical.

Analysis: Figure (19) shows radial and circumferential phase plugs, where N is the number of channels and A is total area.

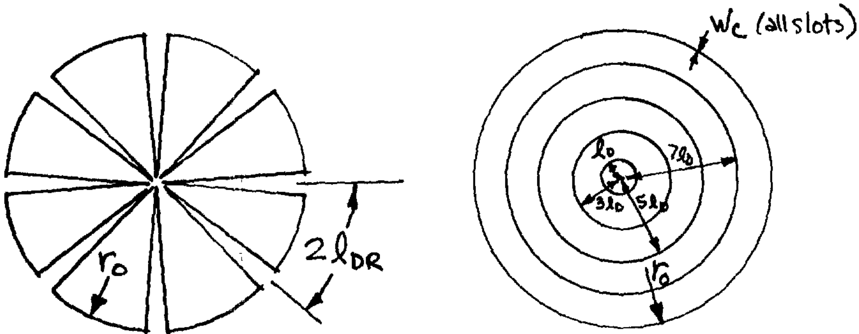

$$A_c = \sum 2\pi \ell_D W_c + 2\pi(3\ell_D)W_c + \ldots.$$

2 slits, $A = 2\pi(4\ell_D)W_c$

3 slits, $A = 2\pi(9\ell_D)W_c$

4 slits, $A = 2\pi(16\ell_D)W_c$; for N_c slits,

Figure (23) - Radial and Circumferential Phase Plugs

$$A_R = N_R\left(\frac{W_R r_o}{2}\right) \qquad (43)$$

$$A_c = 2\pi N_c^2 W_c \ell_D \qquad (45)$$

$$\ell_{DR} = \frac{2\pi r_o}{2N_R} = \frac{\pi r_o}{N_R} \qquad (44)$$

$$\ell_{DC} = \frac{r_o}{2N_c} \qquad (46)$$

$$A_c = \pi N_c W_c r_o \qquad (47)$$

for equal ℓ_D's and areas,

$$\ell_{DR} = \ell_{DC} \therefore \frac{\pi r_o}{N_R} = \frac{r_o}{2N_c} \therefore N_R = 2\pi N_c \qquad (48)$$

$$A_R = A_c \therefore \frac{N_R W_R r_o}{2} = \pi N_c W_c r_o \qquad (49)$$

using (48) and (49) $W_R = W_c$